CIRP Journal of Manufacturing Science and Technology 54 (2024) 1–13

Contents lists available at ScienceDirect

CIRP Journal of Manufacturing Science and Technology

journal homepage: www.elsevier.com/locate/cirpj

On the effect of material density in dimensional evaluations by X-ray computed tomography of metal-polymer multi-material parts

Daniel Gallardo [a,*], Lucía-Candela Díaz [a], Filippo Zanini [b], José Antonio Albajez [a], Simone Carmignato [b], José A. Yagüe-Fabra [a]

[a] I3A, Universidad de Zaragoza, María de Luna 3, Zaragoza 50018, Spain
[b] Department of Management and Engineering (DTG), University of Padova, Stradella San Nicola 3, Vicenza 36100, Italy

ARTICLE INFO

Keywords:
X-ray computed tomography
Multi-material
Dimensional evaluation
Metrology
Polymers
Metal

ABSTRACT

An important aspect to consider in the evaluation of parts and assemblies by X-ray computed tomography (XCT) is the attenuation coefficient of the different materials involved, which are directly related to their density; depending on this coefficient, the X-ray penetration varies and, therefore, varies the contrast between different materials and with the background. This becomes more critical in those assemblies in which materials are characterized by a high difference in density, where the lighter material could be difficult to be characterised. In this paper, the effect of the presence of metals in the dimensional evaluation of polymeric geometries (having lower density than the metal parts) is studied, to evaluate the errors caused in dimensional measurements of different geometries and surface texture characterization. Based on a common geometry, four scenarios have been experimentally tested with variations of metal amount, in which macro geometries (precision spheres made by different polymers) and micro geometries (inclined ramps manufactured by fused deposition modelling (FDM)) have been characterised. Results show errors in the surface determination of the polymeric features directly related to the presence of metal: a high amount of steel makes significantly difficult to accurately determine the interface between background and material due to the noise and artifacts created, while aluminium has less influence on the irregularities of the features extracted. This effect is more evident for polymers with lower density due to the higher difference. Numerically, most affected parameters are those sensible to variations in surface determination, such as spheres' form error and ramps' maximum surface texture (*Sz*), while more solid features as spheres' diameters, distances and ramps' average surface texture (*Sa* and *Sq*) remain more stable. In conclusion and to sum up, it has been found that the quantity of metal present in assemblies made of polymeric and metallic materials is correlated with distortions in the dimensional evaluation of polymeric features by XCT.

1. Introduction

Inspection of parts and assemblies in the field of industry has always been an important aspect in order to ensure the compliance with quality requirements. In terms of dimensional accuracy, different metrological devices and techniques have been developed, each one for a specific purpose: tactile and optical coordinate measuring systems are commonly used for the measurement of macro geometries (basic elements such as cylinders, spheres, planes) and their characteristics (GD&T, dimensions, distances), while optical microscopes as focus variation microscopes (FVM) or confocal microscopes are used for the evaluation of micro geometries (surface topography and geometries with submillimetre dimensions [1]). Therefore, there was a lack of metrological instruments able to characterise different types of geometries simultaneously. This changed when X-ray computed tomography (XCT) started to be applied for industrial metrology [2]. XCT is based on the acquisition of bi-dimensional (2D) projection images (i.e., radiographs) at different angular views of an object, which is typically rotated by 360º, to obtain a complete reconstruction of its three-dimensional (3D) geometry via specifically developed algorithms. Opposite to other 3D technologies, as those mentioned above, it enables the characterization of both accessible and difficult-to-access (e.g., internal) geometries and surfaces of the analysed parts [3,4], being a powerful technique for non-destructive evaluation of components and assemblies

* Corresponding author.
E-mail address: dgallardo@unizar.es (D. Gallardo).

https://doi.org/10.1016/j.cirpj.2024.08.003
Received 9 January 2024; Received in revised form 20 July 2024; Accepted 9 August 2024
Available online 12 August 2024
1755-5817/

with complex geometries [5,6]. In addition, it also allows the inspection of porosity and fractures in objects with no need of destructive operations, such as sectioning [7,8].

XCT working principle relies on the attenuation of the X-rays that pass through the object and are registered by the detector, so one of the main aspects to consider when setting the XCT scanning parameters is the attenuation coefficient of the material [9]. The proportion of rays absorbed by the part and transmitted to the detector depends on such attenuation coefficient, which is directly related to the material density: denser materials as metals need higher energy. In conventional industrial XCT devices, a polychromatic X-ray spectrum is typically employed, including high and low energy rays in the generated beam. The beam hardening is one of the issues found in XCT evaluation, which can cause distortions mainly in metals [10,11]. Physical filters and specific software tools can be used to reduce the beam hardening effect [12]. In order to optimize the quality of an XCT scan, the acquisition parameters (voltage, current, exposition time, etc.) should be adequately adjusted for the specific object of interest [13].

The parameters adjustment becomes more challenging when evaluating assemblies or parts made by two or more materials with different attenuation coefficients [14]. If parameters are adjusted considering the denser material, increasing the energy of the beam, lighter material may not be visible or distinguishable from the air (contrast reduction); on the other hand, a low-energy beam could not be sufficient for passing through the denser material and there would be a high possibility of image artifacts (such as metal artifact) appearance [15].

Several studies have been performed to try to optimise XCT multi material measurements. Two critical aspects that were identified are the surface determination [15] and the thickness of the outer material layer, especially when the denser material is on the outside [16].

For the surface determination, a correct boundary location can be hindered due to the contrast between materials and the image artifacts generated by denser material. Different surface determination algorithms have been studied to determine the most adequate method [16]. Surface determination is in general one of the most relevant factors influencing the accuracy of XCT measurements of dimensions [17,18].

Concerning surface topography measurements, studies have been made for mono-material parts made of polymers [19] and metals [20], in which different techniques are utilised for the extraction and characterisation of the surfaces. However, in multi-material objects, an additional challenge is presented due to the scattered radiation caused by high-density materials. This could blur the boundaries between parts, reduce air-material contrast and, as a consequence, complicate the surface determination. In those cases, algorithms and filters as Gaussian filters [21] are applied for mitigating these effects. In addition, the outer layer thickness can further complicate the dimensional measurement of inner regions when surrounded by denser materials.

A common combination of high-density and low-density materials in industrial assemblies is metal and polymer, as they provide complementary characteristics to the final product (in terms of mechanical and thermal properties, as metals typically present better tenacity and stiffness while polymers are more resistant to external agents which produce corrosion and oxidation). Optimisation of imaging parameters for dimensional XCT measurements on this type of workpieces has been studied [22]. However, as attenuation coefficient has a high affection on XCT evaluation, different materials would still require different adjustments in XCT settings, even for similar workpieces. As mentioned before, polymers as low density materials will be more sensible to this XCT settings adjustment in terms of distortions in dimensional evaluation.

In this paper, a study of the effects caused by metals in the evaluation of polymeric macro and micro features in metal-polymer assemblies by means of XCT is presented. As mentioned before, a material change in the part causes different results, so several scenarios have been considered varying the type and amount of metal present in the metal-polymer test object, which is an assembly designed ad-hoc for the experiment. Metallic inserts (steel screws and bolts) as well as metallic coverings (sheets made by aluminium or steel) are present in the assembly depending on the evaluation scenario. The workpiece includes various polymeric ramps, manufactured by additive manufacturing (AM), with different nominal roughness values as measurands for surface topography characterisation. Polymeric calibrated precision spheres have been included to (i) evaluate the dimensions of diameters, form errors and distances, and (ii) quantify the XCT measurement errors.

2. Materials and methodology

In this section, a description of the study is presented, including the details of the experiments and the scenarios planned (Section 2.1), materials selected for each feature (Section 2.2), methodology followed for the evaluation (Section 2.3) and simulations performed to complete the XCT measurements (Section 2.4).

2.1. Experiments

As the aim of the experiments is to evaluate the effect of metals (high-density materials) in XCT measurements on polymers (low-density materials), various scenarios with different metal proportions have been planned:

– Assembly with no metal (scenario named NM).
– Assembly with metal inserts where polymeric parts are not directly covered. In this case, inserts are screws and bolts (scenario named Scr).
– Assembly with metal coverings that hide polymeric measurands:
  o Low-density metal coverings – aluminium (scenario named Al).
  o High-density metal coverings – steel (scenario named St).

A test object has been designed according to the scenarios planned (see Fig. 1). Moreover, the design was conceived to enable both XCT measurements and reference measurements using conventional metrological devices (see Section 2.3 for more details on the reference measurements).

The main base is designed and manufactured in polyethylene terephthalate glycol (PETG) by filament-based material extrusion (MEX) technology, with orthogonal shape and rounded corners, and general dimensions of 55 mm × 40 mm × 17 mm. The size of the assembly is intended to be as compact as possible but including large enough measurands. The main base is divided into two halves to ease the reference measurements of the precision spheres; both parts of the base are mounted together for XCT evaluation.

Two sets of ramps are included in the base: four upper ramps, designed as a part of the upper base (Fig. 1a), two with an angle of inclination of 20º and two with 40º, and three lower ramps, printed separately at an angle of inclination of 30º and stuck into the lower base (Fig. 1b) in the holes designed for their placement. With this range of angles of inclination of the ramps (20º - 30º - 40º), and a constant layer thickness used for the manufacturing of the parts (0.15 mm), the expected surface texture (*Ra*, *Sa*) for the surfaces evaluated is in a range of 20 – 30 μm according to predictive models [23,24].

Four commercial precision spheres of 12 mm in diameter are located in the base as seen in Fig. 1a, placed as vertex of a square with a distance of 18 mm between each sphere. Each sphere is made of a different polymeric material: polypropylene (PP), Nylon (PA6.6), polyoxymethylene (POM) and Teflon (PTFE).

Two types of metal coverings are designed: aluminium plates (low-density metal, thickness of 3.85 mm) and steel plates (high-density metal, thickness of 2 mm) with the same shape as the main base. For each scenario, two metallic parts of the same material are used (one placed over the upper base and one placed under the lower base).

Screws and bolts are used for fixing the assembly. The material used for the fixture objects included in the no-metal assembly is PA6.6, while

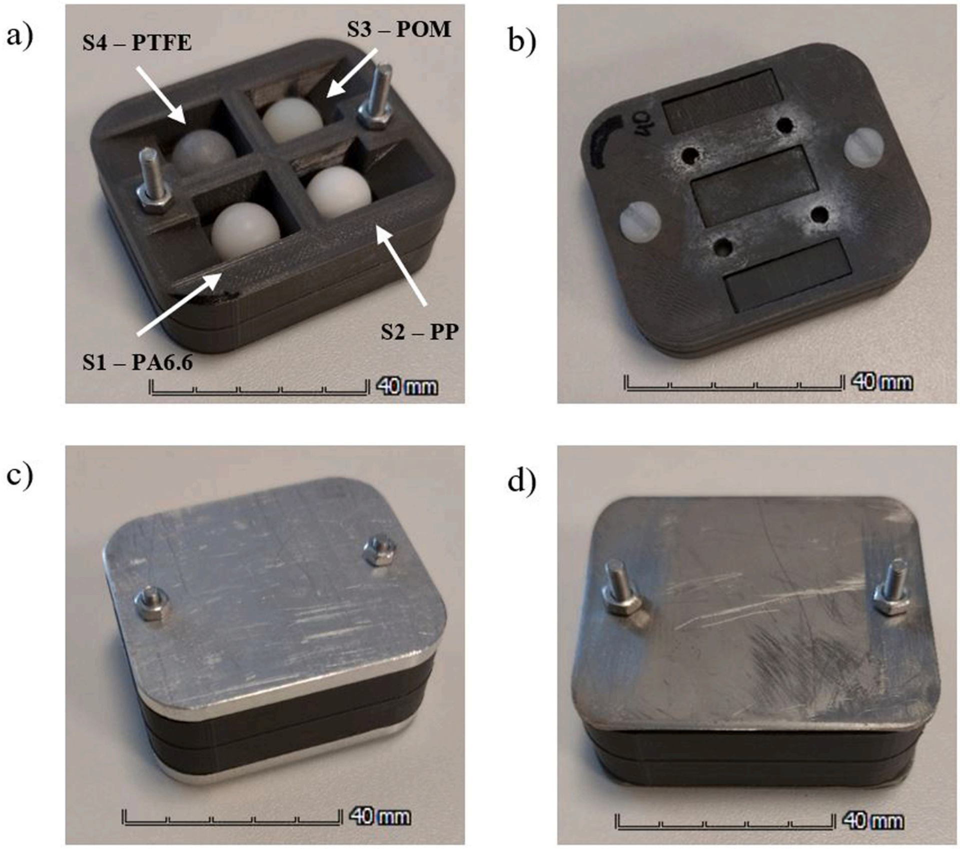

Fig. 1. Metal-polymer assembly. a) With metal inserts (upper view). b) No metal (lower view). c) Aluminium plates. d) Steel plates.

in the rest of the scenarios the chosen material is steel. In the assembly with metal inserts, screws and bolts also play the role of metal inserts. In Fig. 2, the distribution of the elements in the CAD model is shown.

2.2. Material selection

In Table 1, a summary of the materials used for each part and its density is presented.

Table 1
List of materials used and corresponding density.

Material	Parts	Density (g/cm^3)
Polyethylene terephthalate glycol (PETG)	Main base, polymeric screws and bolts.	1.27
Polypropylene (PP)	1 precision sphere (S2)	0.87
Nylon (PA6.6)	1 precision sphere (S1)	1.11
Polyoxymethylene (POM)	1 precision sphere (S3)	1.37
Teflon (PTFE)	1 precision sphere (S4)	2.16
Aluminium (Al)	Metal plates	2.70
Steel	Metal plates, metal screws and bolts.	7.85

2.3. Evaluation

In Fig. 3, a summary of the workflow followed for the measurements is shown.

Reference measurements have been taken prior to XCT evaluation:

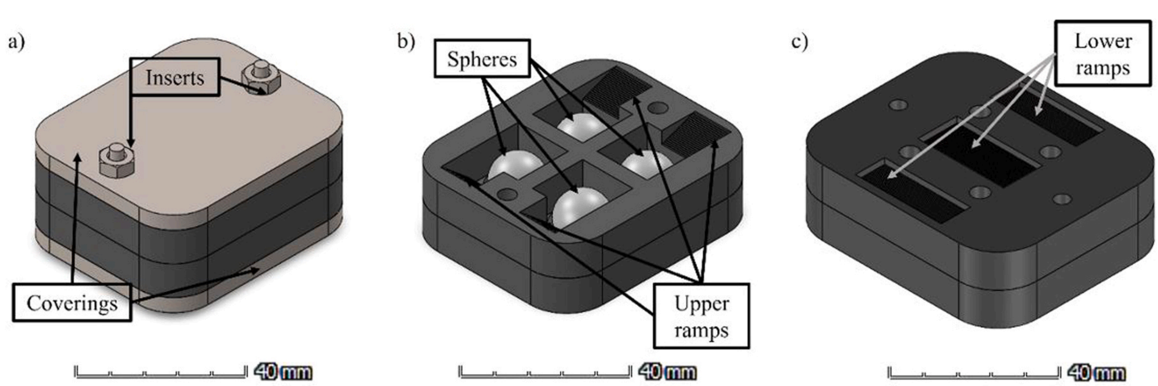

Fig. 2. CAD model and element distribution. A) Complete assembly. B) Top face. C) Bottom face.

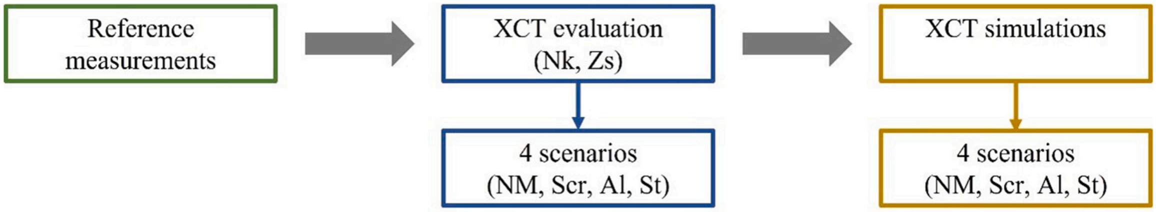

Fig. 3. Methodology workflow followed in the experiment.

– Spheres were measured by a coordinate measuring machine (CMM) ZEISS PMC-876 CNC, with a 3 mm in diameter spherical ruby probe. Expanded uncertainty results registered are in a range of U_{CMM} = 2.4-2.6 µm for diameters and distances and U_{CMM} = 2.1-2.2 µm for spheres form error.
– Ramps have been characterized by a focus variation microscope InfiniteFocusSL of Alicona. A 10 × magnification lens was used, with a lateral resolution of 8 µm and a vertical resolution of 130 nm. STL files were exported for each ramp. Expanded uncertainty results registered are in a range of U_{FVM} = 2-3 µm for *Sa* parameter.

Two different devices have been used for the XCT measurements: a Zeiss Metrotom 1500 (Zs in the results) and a Nikon Metrology MCT225 (Nk in the results). Performance verification of the devices has been done according to the guideline VDI/VDE 2630 Part 1.3 [25]; this protocol, along with the geometrical and thermal stability systems present in both devices, ensures that scaling errors are minimized, preventing unnecessary re-scaling of the voxel size [26]. Settings were optimized and three iterations have been performed for each device and for each scenario; values are presented in Table 2.

Post processing has been performed with the software VG Studio Max 3.4.2 (Volume Graphics GmbH, Germany). First general surface determination (SD) has been made in Advanced – multi material mode, with a differentiation between polymers in no metal scenarios and differentiation between polymers and metals in the rest of the cases; a search distance equal to 4 times the voxel size has been selected. Regions of interest (ROIs) have been created for each element (4 spheres, upper ramps lower ramps) and a second local SD for each ROI has been done using the same parameters. Multi material differentiation has been made in local SD when applicable. Uncertainty estimations have been done according to guidelines (see Section 3.2.2 and VDI/VDE 2630 Part 2.1).

2.4. Simulations

In addition to the XCT measurements, XCT simulations have been performed by the software aRTist 2.12 (BAM, Germany). One simulation has been made for each scenario (see Section 2.1). Settings of the simulations have been used also to adjust the parameters utilized for scanning with the Nikon Metrology MCT225 system, as it was possible to access directly to the device; on the other hand, as Zeiss tomographies have been made in an external laboratory, not all necessary data to simulate the process were available. The selected measurands of the simulation results are the diameters, distances and form errors of the spheres, which have been evaluated and compared to the real XCT results.

3. Results and discussion

In this section, details of the results obtained in the evaluation are presented, including general remarks about the tomographies and the contrast between materials (Section 3.1), results related to the spheres measurements (Section 3.2) and surface texture characterisation (Section 3.3). Finally, discussion of the results is added in Section 3.4.

3.1. Image contrast

In Figs. 4, 2D slices of each XCT scenario are displayed. Slices are longitudinal to the ramps and focused on the central ramp and fixtures (screws and bolts).

The contrast between denser elements (brighter) and lighter parts (darker) is shown in Fig. 4. Contrast between background and polymer is clear in no metal (NM) scenario (Fig. 4a). High metal artifacts and noise levels were found in the assembly with steel coverings (St) (Fig. 4d), creating difficulties to differentiate between background and polymer. In the remaining tomographies (Scr, Al), the presence of metal has less impact in the contrast background – polymer, therefore allowing to observe and characterise the threshold with an acceptable clearance.

To numerically validate the trend suggested by the X-ray slices, contrast-to-noise ratio (CNR) has been calculated from the gray value data obtained in software VG Studio Max 3.4.2 (Volume Graphics GmbH, Germany), following the procedure described in [27], using Eq. 1:

$$CNR = \frac{\left|A_{Material} - A_{Background}\right|}{\sqrt{\sigma^2_{Material} + \sigma^2_{Background}}} \quad (1)$$

where $A_{Material}$ and $\sigma_{Material}$ represent the mean and standard deviation of the material ROIs, respectively; $A_{Background}$ and $\sigma_{Background}$ represent the mean and standard deviation of the background ROIs, respectively.

In Table 3, CNR values and peak difference (material-background) obtained for the gray value analysis of the polymeric base (ROI of the material separated from the metal).

Results confirm that contrast between polymer elements and background (air) is significantly lower in scenario with steel coverings (St). Values found in the rest of scenarios are similar, observing slight less contrast in Scr and Al scenarios; this suggests that presence of a higher amount of steel affects considerably the quality of the tomographic reconstruction, but it is not the case of aluminium.

Table 2
Parameters used for each XCT measurement.

Parameter	Nk NM	Nk Scr	Nk Al	Nk St	Zs NM	Zs Scr	Zs Al	Zs St
Voltage/kV	130	215	215	220	140	140	195	175
Current/µA	108	75	75	73	410	410	294	328
Physical filter	-	Cu 0.5 mm	Cu 0.5 mm	Cu 0.85 mm	Al 2.0 mm	Al 2.0 mm	Cu 0.75 mm	Cu 0.75 mm
Projections	1500	1500	1500	1500	1500	1500	1500	1500
Exposure time/ms	1000	1420	1420	2000	500	500	500	500
Voxel size/µm	36.02	36.02	36.02	36.02	47.56	47.56	47.56	47.56

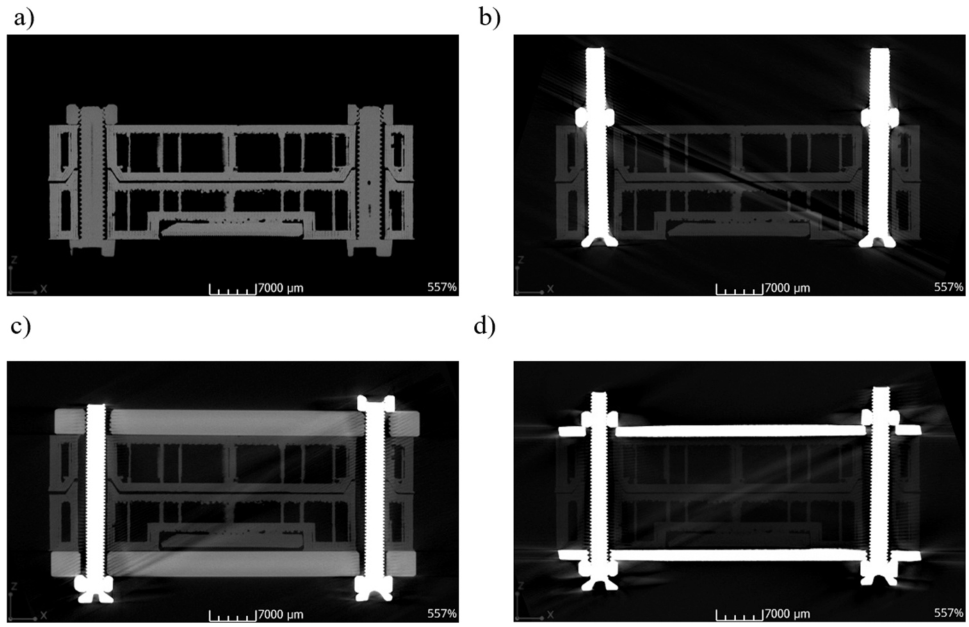

Fig. 4. - X-Ray slices of XCT reconstruction. a) No metal. b) Steel inserts added. c) Aluminium coverings. d) Steel coverings.

Table 3
CNR results for polymeric ROIs in each scenario.

Scenario	Peak difference (A_M-A_B)	CNR
NM	2793.33	2.18
Scr	1021.37	2.13
Al	1638.92	2.01
St	1162.31	0.92

3.2. Spheres

In this section, a summary of the results obtained by the evaluation of dimensional features of the spheres and the data found in the XCT histograms is presented.

3.3. Numerical comparison

Diameter, form error and distances between spheres have been obtained and compared, registering mean values of the measurements for each feature. A search distance has been established for all macro geometries in 200 µm. A quality threshold of 2σ (95 %) of the points registered has been used, to reduce overestimation of form errors caused by aberrations. For graphics of diameters and form errors, density has been considered for comparison in the *x* axis; a vertical red line has been included in diameters and form errors graphics representing the density of the material of the base.

A summary of the absolute form error of the four spheres for each scenario and each evaluation is shown in Fig. 5, including the results obtained by using the CMM and results obtained in simulations. Deviations of XCT diameter values from CMM measurements are shown in

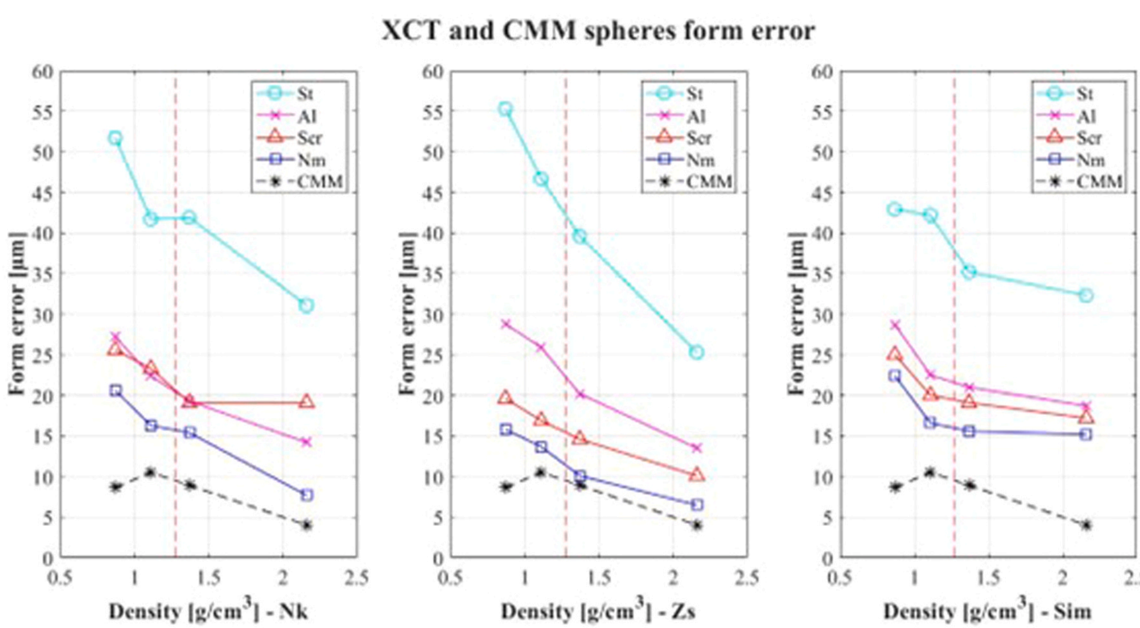

Fig. 5. Form error of polymeric spheres for each scenario in XCT measurements, simulations and CMM.

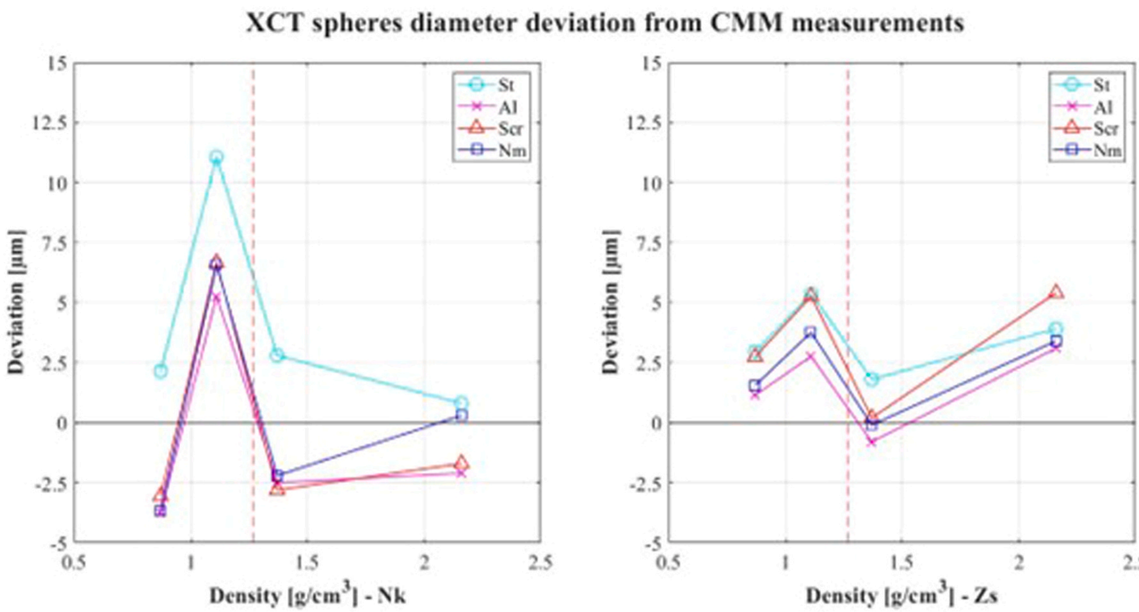

Fig. 6. Mean deviations of diameters and distances from NM scenario.

Fig. 6, and deviations of XCT distances between spheres values from CMM measurements are shown in Fig. 7.

Higher form errors were found in scenarios with higher amount of metal, mainly in St scenario (steel fixtures and plates). A trend is also observed regarding the density of the sphere's material: as the density increases, form error decreases. It suggests that even for the NM scenario where noise is significantly lower, differences in density between materials causes that an optimisation of XCT settings favours the denser material, at least for highly surface determination dependant features as form error. This tendency is not observed in diameters and distances; similar results are obtained in each sphere for diameters, while the deviations distribution for distances seems more random. The reason is that both diameters and distances are not as dependant on surface determination and external noise as form error. Simulations also confirm such observations; but results in simulated and real tomographies are slightly different. Distances and diameters obtained in simulations are not used for comparisons, as in simulation the measurand is the CAD model and, therefore, manufacturing deviations of the real part are not considered.

Regarding reference measurements, higher form error in XCT is found compared to CMM. Different measuring principles are used for each technology; XCT surface determination allows to obtain a more detailed characterisation of the features in terms of points acquired while accuracy of the measurements is better for CMM since uncertainties are in general lower. Profile filtration is also different: CMM resolution is limited by the diameter of the probe [28], causing a mechanical filtering when reaching deep valleys of the surface, while in XCT it is limited to the achieved magnification (voxel size).

3.4. Measurement compatibility and uncertainty calculations

For the evaluation of the measurement compatibility between XCT

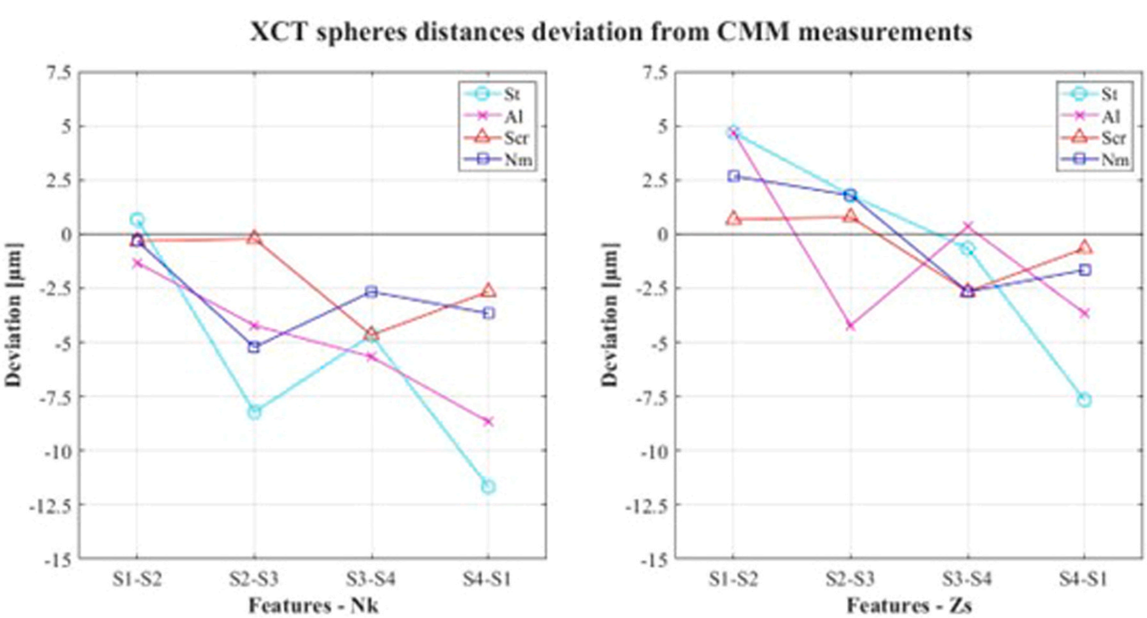

Fig. 7. Deviation of XCT measurements of distances between spheres from CMM measurements.

and CMM measurements, the E_N parameter is calculated, according to normative ISO/IEC 17043:2023 [29], following the equation:

$$E_N = \frac{|y_{XCT} - y_{CMM}|}{\sqrt{U_{XCT}^2 + U_{CMM}^2}} \tag{2}$$

Where y_{XCT} = current measured value of the feature, y_{CMM} = reference value of the feature, U_{XCT} = expanded uncertainty of the XCT measurement and U_{CMM} = expanded uncertainty of reference value. Results are considered valid for $E_N \leq 1$ as stated in the normative.

Uncertainty calculations have been done following the procedures indicated in normative:

- ISO 15530-3:2011 [30] for reference CMM measurements. Expanded uncertainty results registered are in a range of U_{CMM} = 2.4-2.6 µm for diameters and distances and U_{CMM} = 2.1-2.2 µm for spheres form error.
- VDI/VDE 2630-2.1 [31] for XCT measurements, also following the recommendations suggested in [32]. This normative is commonly used for this type of measurements [33,34]. Expanded uncertainty results registered are in a range of U_{XCT} = 12-13 µm for diameters and distances and U_{XCT} = 6-7 µm for form error.

For both devices, coverage factor for the expanded uncertainty calculations is k = 2 for a 95 % confidence interval.

In Table 4, E_N results obtained for each feature and in each scenario are shown. Features evaluated are diameters (*Sx*), form errors (*EFx*) and distances (*Sx-Sx*).

Values of $E_N > 1$ are highlighted in bold, as they are not considered acceptable; also, values of $0.75 < E_N < 1$ are marked with an asterisk because although values are valid, they approach 1.0 and therefore have to be taken with caution. Results show that all values for diameters and distances are valid and almost all are not close to 1, while in form errors only NM scenarios have valid results. However, *EF2* show higher E_N value mainly because, as shown in Fig. 5, it has higher form error due to its lower density. Also, E_N value increases for scenarios with higher amount of metal, which is related with higher form errors as stated in Section 3.2.1.

3.5. Material differentiation

In Fig. 8, grayscale histograms of the ROI of the four spheres in each scenario are displayed. Each peak is labelled in Fig. 8a with its corresponding sphere.

Histograms of ROI extracted of the four spheres show a variation on the distribution of the grey values: the more metal is present in the tomography, the more diffused is the boundary between the peaks of the materials; the most extreme case is St (Fig. 8d) where even the background peak is not distinguishable. This clearly indicates that the denser material decreases the contrast between the lighter materials. However, a good polymer differentiation is possible with the presence of a certain amount of metal in XCT evaluation. As the density of aluminium is significantly lower than the density of steel, it affects less to the characterisation of the geometries, as seen in Fig. 4.

3.6. Inclined ramps

3.6.1. Surface comparison – irregularities

For each XCT measurement, STL files are extracted from each surface and false colour height maps of an 8 × 8 mm area are created. Examples of this features are displayed in Fig. 9a for NM scenario, Fig. 9b for Scr scenario and Fig. 9c for Al scenario. Noise created by steel inserts and coverings in XCT evaluation made not possible to obtain proper surfaces of the ramps in St scenario.

Ramps displayed have an angle of inclination of 30°. Irregularities in the surface extracted become more evident when the metal quantity is increased in the assembly. For a more detailed analysis, individual profiles of each STL shown previously are extracted and displayed in Fig. 10.

When observing profiles, it is clearer that the shape is more irregular for metal scenarios (Scr and Al). However, peaks and valleys remain visible, suggesting that although the presence of noise in the tomographies, profiles for surface texture evaluation are feasible to obtain. To verify it, surface texture parameters *Sa*, *Sq* and *Sz* have been computed. In Annex A, primary profile along with waviness and roughness profiles filtered according to Section 3.3.2 are displayed.

3.6.2. Reference measurements

A first evaluation of the measurands has been done with the FVM reference device (see Section 2.3). XCT scenario selected for the comparison has been NM (no metal), as no distortion caused by metals is present. Areal parameters used for the numerical comparison of ramps have been *Sa*, *Sq* and *Sz*.

Three areas of 4 × 4 mm along each ramp have been measured. L-filter nesting index (hi-pass filter) of 2.5 mm and a S-filter nesting index (low-pass filter) of 8 µm were selected according to normative UNE-EN ISO 25178–3 [35].

As the nominal parameters' values of each ramp are different, percentual deviations have been calculated to equalize the results. Reference measurements are shown in Fig. 11.

Sa and *Sq* values follow the same trend in both devices, having found a negative difference in Zeiss machine. The main reason is the worse geometrical magnification obtained, causing a less precise resolution and, therefore, smoother surfaces; however, negative deviations are not too high (in the range of 10–15 % maximum). Deviations found in *Sz* values are higher, more randomly distributed and almost all negative; this indicates that some peaks/valleys have not been characterised properly as expected by XCT due to its lower resolution than FVM (in

Table 4
E_N parameter for each feature and scenario.

	Zs				Nk			
Feature	NM	Scr	Al	St	NM	Scr	Al	St
S1	0.309	0.426	0.222	0.415	0.551	0.546	0.418	0.894 *
S2	0.131	0.224	0.104	0.360	0.336	0.247	0.293	0.167
S3	0.008	0.016	0.054	0.155	0.174	0.237	0.207	0.215
S4	0.277	0.441	0.256	0.324	0.014	0.139	0.182	0.057
EF1	0.469	0.930 *	**2.268**	**5.453**	0.781 *	**1.380**	**1.268**	**4.576**
EF2	**1.049**	**1.603**	**2.946**	**6.832**	**1.634**	**1.926**	**2.137**	**6.327**
EF3	0.173	0.830 *	**1.639**	**4.481**	0.915 *	**1.134**	**1.119**	**4.839**
EF4	0.361	0.890 *	**1.395**	**3.145**	0.533	**1.773**	**1.160**	**3.988**
S1-S2	0.197	0.074	0.319	0.319	0.025	0.025	0.098	0.098
S2-S3	0.131	0.057	0.311	0.156	0.335	0.041	0.336	0.655
S3-S4	0.147	0.172	0.003	0.025	0.172	0.344	0.393	0.369
S4-S1	0.147	0.049	0.295	0.614	0.270	0.197	0.639	0.836 *

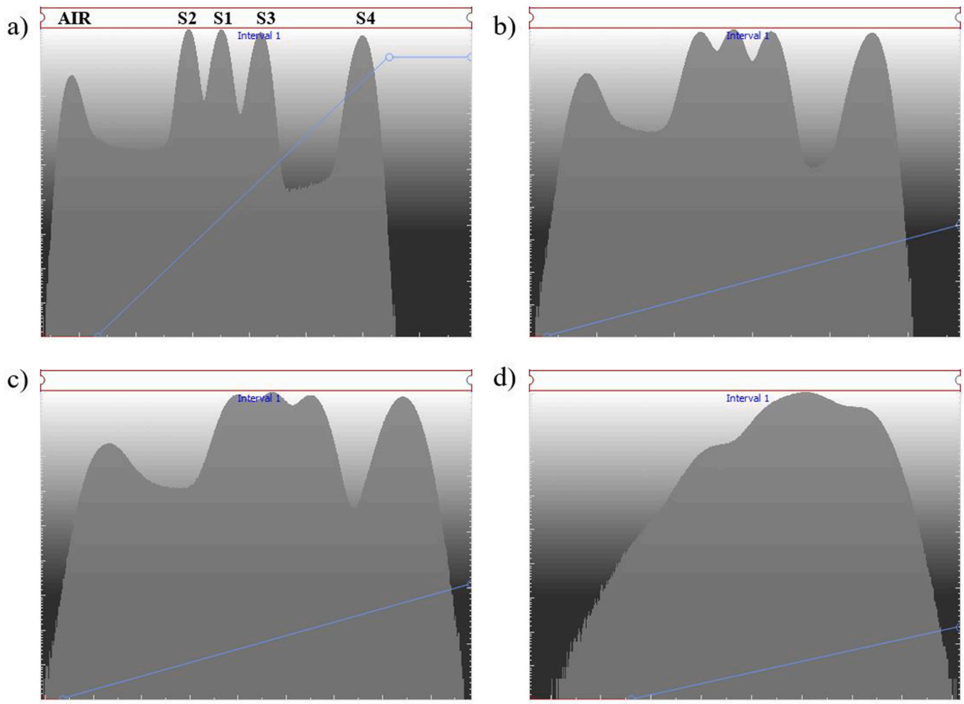

Fig. 8. Grayscale histograms of spheres' ROI. a) NM. b) Scr. c) Al. d) St.

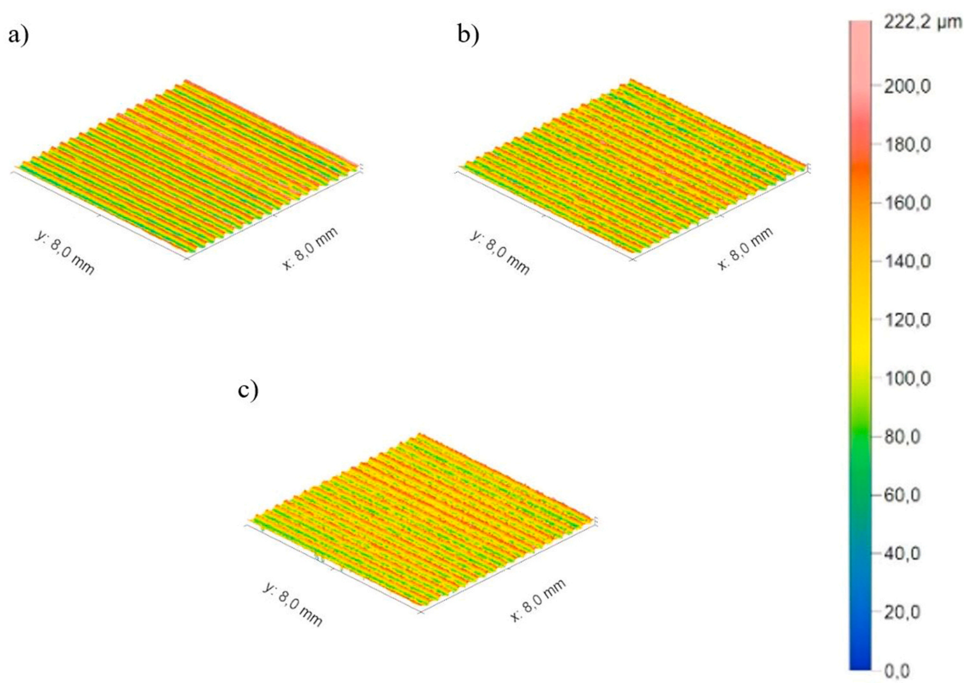

Fig. 9. False height colour maps of STL extracted. a) NM. b) Scr. c) Al.

both XCT devices). However, as the main objective is to compare different XCT scenarios mutually, this comparison XCT-FVM has been done just to be aware of possible errors that occur in the main scenario (no metal, NM).

3.6.3. *Surface texture comparison*

As stated in Section 3.3.2, to equalize the results of all ramps, percentual deviation from reference scenario (NM) has been calculated. Nikon device results are shown in Fig. 12 and Zeiss device results are shown in Fig. 13.

Results show that maximum deviations in *Sa* and *Sq* are in the + /- 15 % range for both scenarios. It indicates that amplitude of the surface texture profile is not highly affected by the noise created by metal added, and therefore with the same resolution of the XCT evaluations (geometrical magnification), acceptable values of average surface texture may be obtained. Regarding *Sz*, as irregularities are present in the ramps in scenarios with metal, errors such as empty regions or spikes could appear and create more random variations in the results since this parameter is much more sensible to abrupt changes in the surface.

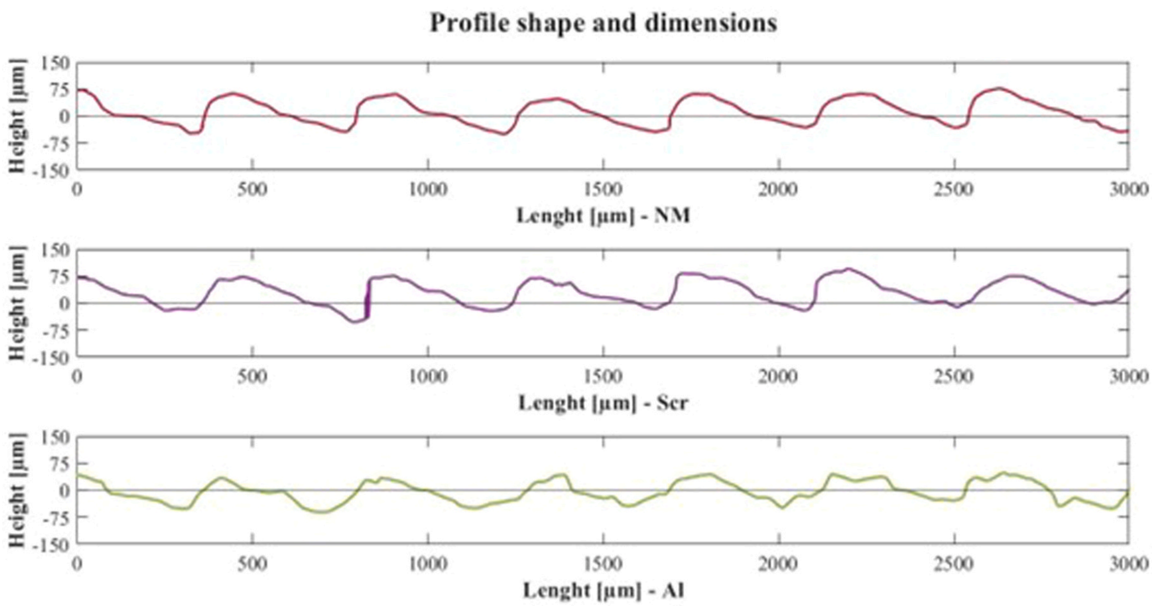

Fig. 10. Individual profiles extracted from the ramps' STL.

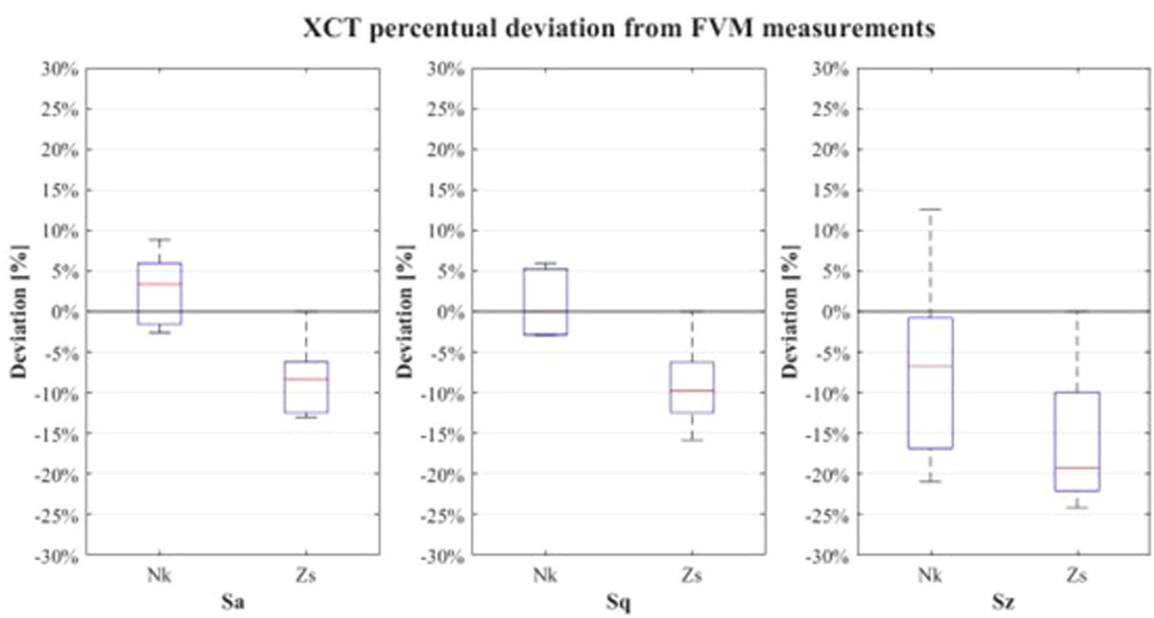

Fig. 11. Mean values of inclined ramps deviations from reference measurements.

3.7. Discussion

In general, results show a correlation between less accurate surface obtained on the polymeric features by XCT and quantity of metal present in the XCT characterisation. Numerical results show higher deviations in features where surface determination has a high influence (as form error and maximum surface texture *Sz*); however, for diameters, distances and average values of surface texture (*Sa*, *Sz*), whose value is more independent to the obtained surface, variations found are in an acceptable range according to the measurement comparability parameter calculation (E_N) based on uncertainty calculations.

Focusing on highly influenced parameters, it is clear that noise created by the presence of metal artifacts in the XCT characterisation affects the variations in both form error and maximum surface texture *Sz* proportionally. Scenario with steel plates has been the most conflictive to obtain a proper surface determination: spheres evaluation has been possible with important distortions, while boundaries between ramps and background were not sufficiently clear to adequately extract the features. Logical reason is the high density of the metal and the high contrast with the polymers, and low contrast between polymer and air. Nevertheless, it has been demonstrated that when the amount of steel is not high (as in Scr and Al scenarios, where steel is only present as inserts), the level of noise and artifacts does not prevent from obtaining accurate dimensional results. Other important aspect is that, for this moderate quantity of metal, it has been possible to differentiate between polymers with similar density with an acceptable accuracy (Fig. 8).

On the other hand, influence of aluminium has been much lower. Al plates create distortions, but the influence of the steel inserts was higher; differences between Al and Scr scenarios were much lower than between Scr and NM. The suggestion is that the lower density of this material

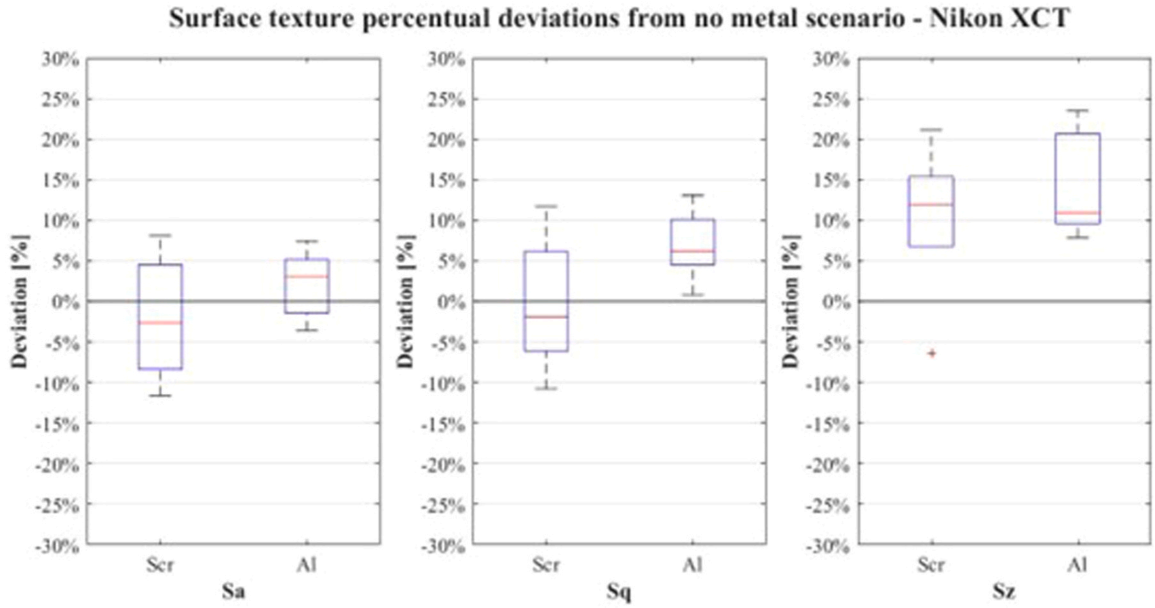

Fig. 12. Nikon device XCT surface texture results.

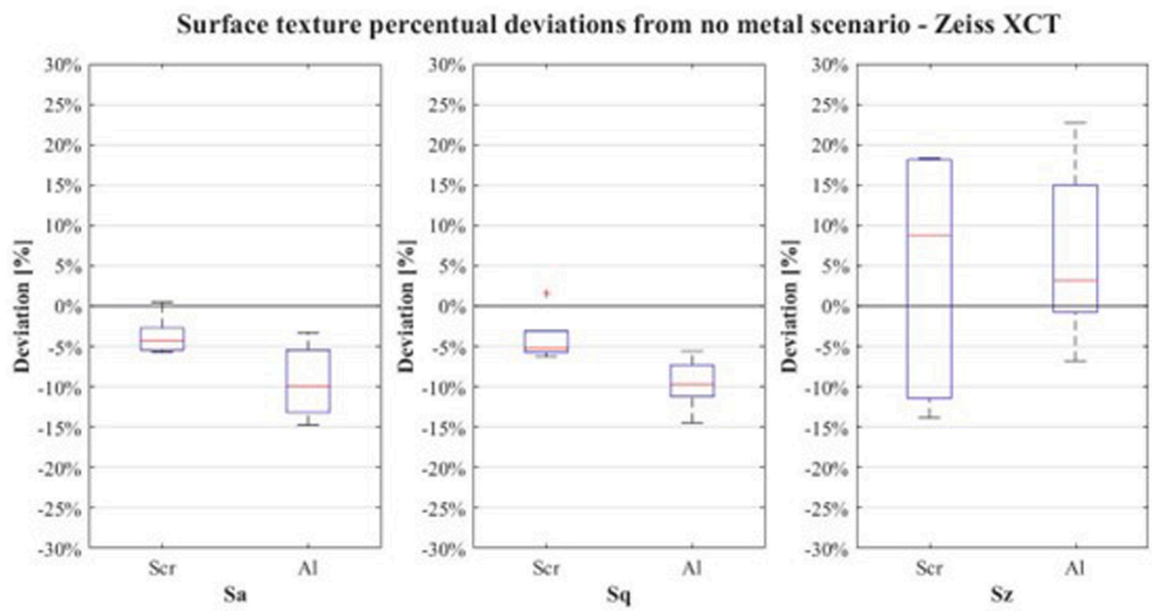

Fig. 13. Zeiss device XCT surface texture results.

comparing to steel and its closer value to the polymers' density are the main reasons for these results.

Additionally, it has been found that density of the polymer also creates different deviations in the spheres, as the optimisation of the XCT parameters for the correct measurement of polymers also favour the denser ones. All tomographies follow the same trend; lighter material, higher form error, affected proportionally depending on the amount of metal present.

4. Conclusions and future work

In this paper, an evaluation of the influence of denser materials such as metallic parts on dimensional measurements by XCT of polymeric features in metal-polymer assemblies is presented. Polymeric macro and micro geometries are included as measurands in an ad hoc designed test object, previously measured with reference devices, and four different scenarios have been planned with variations in the amount and type of metal present (considering aluminium and steel for the study). The objective of the workpiece design has been to i) simplify the design and to ii) equalize the number of projections affected by metal elements. As the aim is to evaluate exclusively the differences in the results of dimensional evaluation of polymeric features produced by the introduction of metallic elements, XCT parameters and post processing of the reconstructed volume has been optimized for each scenario as it is usually done in common XCT measurements.

Results quantified the correlation between the amount of metal present in the assembly and the deviations of the XCT evaluation with respect to the no metal scenario. These deviations are more relevant for measurands that are sensible to changes in surface determination: spheres' form error and maximum surface texture *Sz*. Diameters,

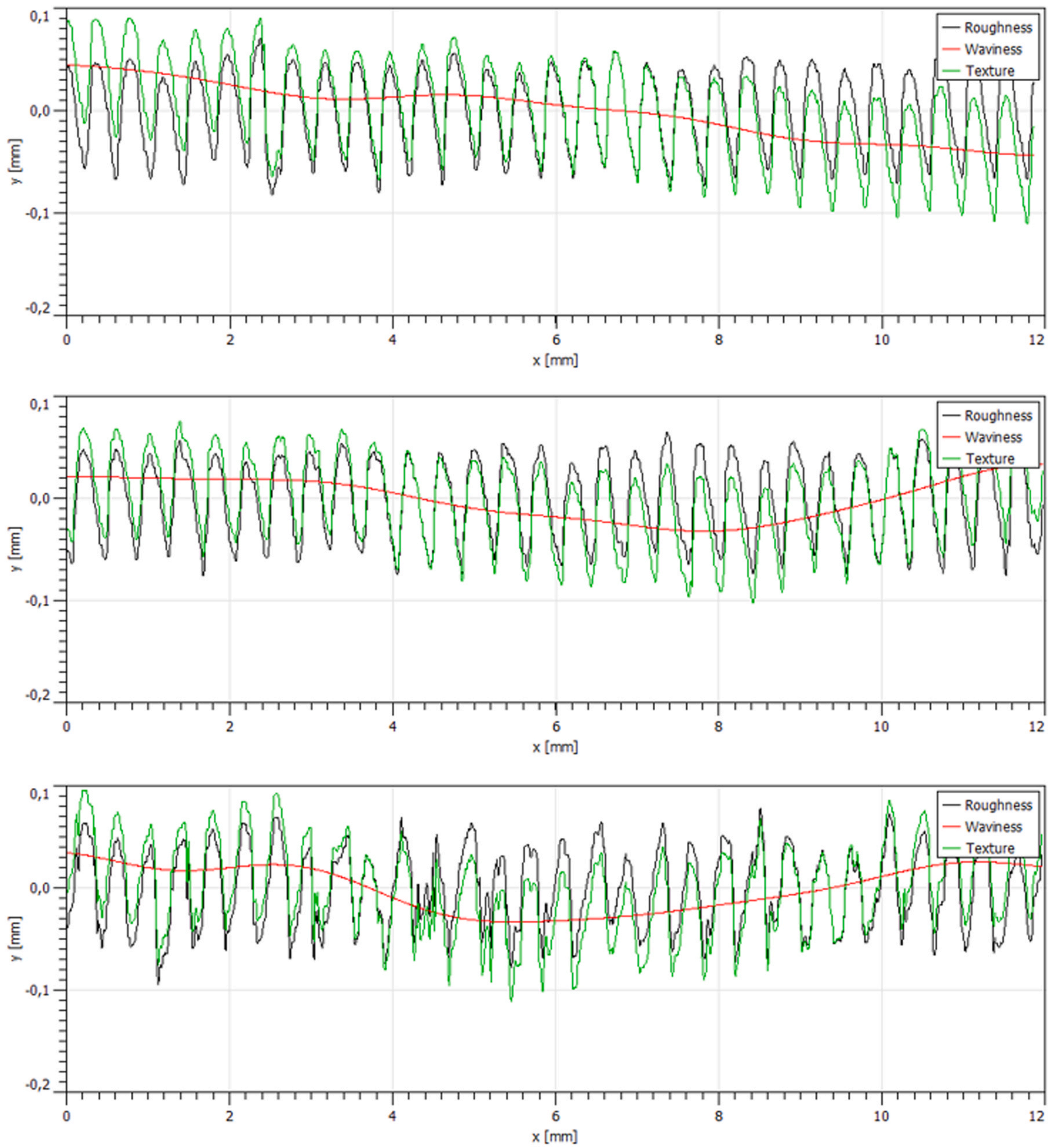

Fig. 14. Roughness, waviness and texture profiles obtained by Nikon device for each scenario. a) NM. b) Scr. c) Al.

distances and average surface texture (*Sa* and *Sq*), as less surface-dependent features, are less affected by the variations caused by metals. Visually, it is possible to observe the irregularities created in the surface extracted from the inclined ramps; this confirms together with the dimensional macro and micro evaluation the higher deviations caused by metals.

Due to its high density difference, and therefore high attenuation coefficient, increasing the amount of steel significantly hinders the surface determination of the polymeric features, creating a high amount of noise and image artifacts that amplify form error evaluated on the spheres and makes it impossible to characterise properly the ramps. On the other hand, good results have been achieved in Scr and Al tomographies (steel inserts and steel inserts with Al coverings, successively), even being able to differentiate between polymers with similar densities. It indicates that aluminium effect on the polymeric parts is lower, mainly because its attenuation is also lower than steel. Also, lighter polymers in multi-polymeric assemblies are affected by the noise created by denser polymers, even though the effect is smaller.

With this investigation, better knowledge regarding metal influence on the evaluation of polymeric macro and micro geometries is provided. Although this study is focused on a particular designed test object, some tendencies are identified but results may vary for different configurations, geometries, amount of metal and materials used. For future work, the objective is to extend the range of the experiment, varying parameters such as thickness of metal sheets, part geometry, percentage of XCT projections affected by metal, and including other metals with different attenuation coefficients.

CRediT authorship contribution statement

Daniel Gallardo Artal: Conceptualization, Formal analysis, Investigation, Methodology, Validation, Visualization, Writing – original draft. **Filippo Zanini:** Conceptualization, Resources, Supervision, Writing – review & editing. **Lucía-Candela Díaz:** Conceptualization,

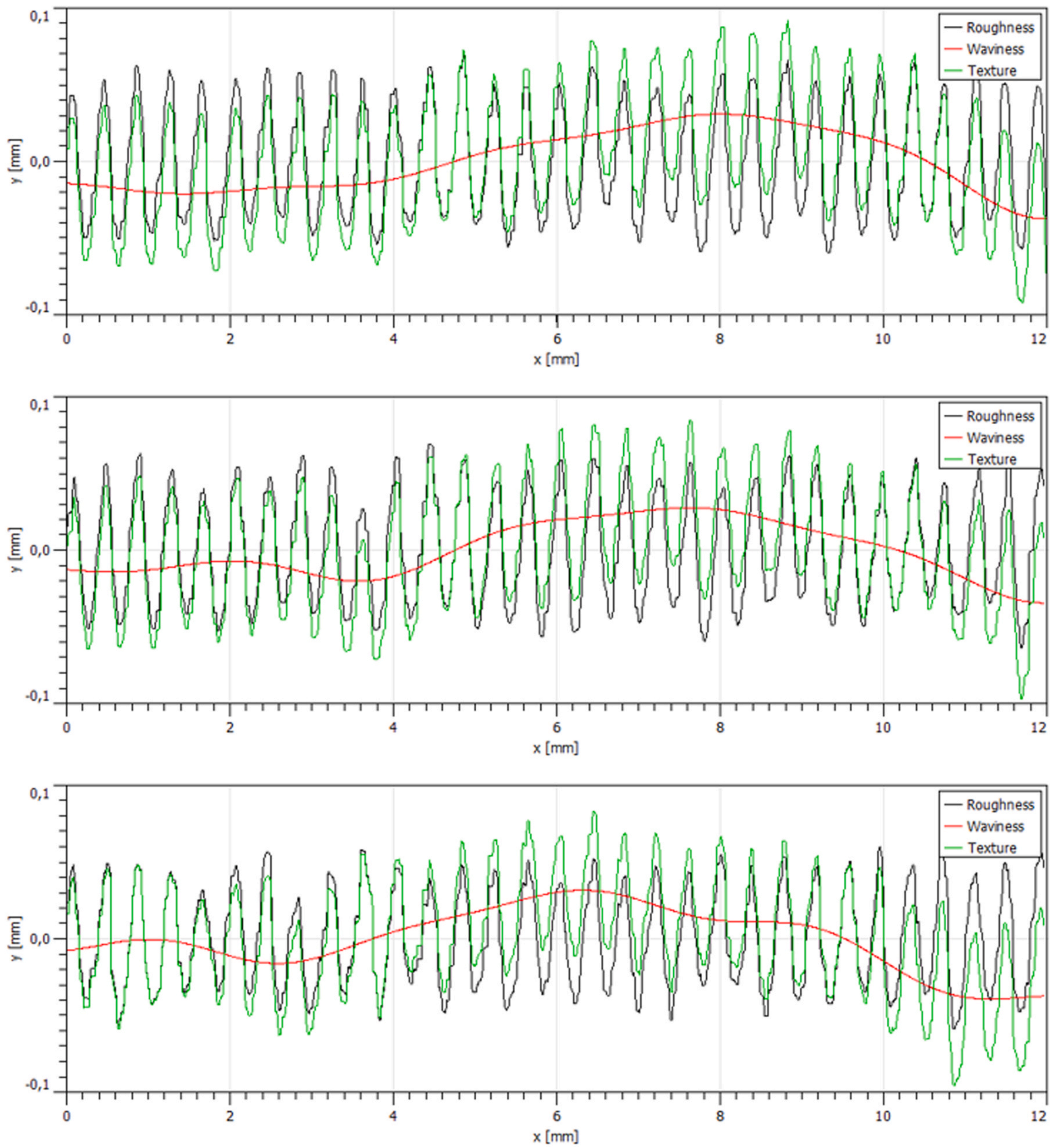

Fig. 15. Roughness, waviness and texture profiles obtained by Zeiss device for each scenario. a) NM. b) Scr. c) Al.

Resources, Supervision, Writing – review & editing. **Simone Carmignato:** Funding acquisition, Project administration, Supervision, Writing – review & editing. **José Antonio Albajez:** Conceptualization, Funding acquisition, Project administration, Resources, Supervision, Writing – review & editing. **José Antonio Yagüe-Fabra:** Funding acquisition, Project administration, Supervision, Writing – review & editing.

Declaration of Competing Interest

The authors declare that they have no known competing financial interests or personal relationships that could have appeared to influence the work reported in this paper.

Acknowledgements

This work was supported by project RTI2018–097191-B-I00 funded by MCIN/AEI/10.13039/501100011033 and by ERDF A way of making Europe; by project PID2021–127134O-B-I00 funded by MCIN/AEI/10.13039/501100011033 and by ERDF A way of making Europe; and by grant PRE2019-089465 funded by MCIN/AEI/10.13039/501100011033 and by ESF Investing in your future.

Annex A: Roughness and waviness profiles for XCT ramps

In this annex, primary profile (texture), roughness and waviness of a 30º ramp are displayed, for each scenario and each XCT device.

References

[1] Triantaphyllou A, Giusca CL, Macaulay GD, Roerig F, Hoebel M, Leach RK, et al. Surface texture measurement for additive manufacturing. Surf Topogr 2015;3. https://doi.org/10.1088/2051-672X/3/2/024002.

[2] Villarraga-Gómez H, Herazo EL, Smith ST. X-ray computed tomography: from medical imaging to dimensional metrology. Precis Eng 2019;60:544–69. https://doi.org/10.1016/j.precisioneng.2019.06.007.

[3] Jansson A., Reza Zekavat A., Pejryd L. Measurement of Internal Features in Additive Manufactured Components by the use of Computed Tomography Measurement consistency in X-ray computed tomography View project MultiMatCT View project. 2015.
[4] McGregor DJ, Bimrose MV, Tawfick S, King WP. Large batch metrology on internal features of additively manufactured parts using X-ray computed tomography. J Mater Process Technol 2022;306. https://doi.org/10.1016/j.jmatprotec.2022.117605.
[5] Praniewicz M, Fox J, Ameta G, Kim F, Witherell P, Saldana C. Exploring registration of optical, CMM and XCT for verification of supplemental surfaces to define AM lattices: application to cylindrical and spherical surfaces (Elsevier B.V) Procedia CIRP 2020;vol. 92:181–6. https://doi.org/10.1016/j.procir.2020.05.182.
[6] Zanini F, Sorgato M, Savio E, Carmignato S. Dimensional verification of metal additively manufactured lattice structures by X-ray computed tomography: Use of a newly developed calibrated artefact to achieve metrological traceability. Addit Manuf 2021;47. https://doi.org/10.1016/j.addma.2021.102229.
[7] Hermanek P, Carmignato S. Reference object for evaluating the accuracy of porosity measurements by X-ray computed tomography. Case Stud Nondestruct Test Eval 2016;6:122–7. https://doi.org/10.1016/j.csndt.2016.05.003.
[8] Jin J, Lin CL, Assemi S, Miller JD, Butt DP, Jordan T, et al. Nanopore networks in colloidal silica assemblies characterized by XCT for confined fluid flow modeling. J Pet Sci Eng 2022;208. https://doi.org/10.1016/j.petrol.2021.109780.
[9] Ma X, Buschmann M, Unger E, Homolka P. Classification of X-ray attenuation properties of additive manufacturing and 3D printing materials using computed tomography from 70 to 140 kVp. Front Bioeng Biotechnol 2021;9. https://doi.org/10.3389/fbioe.2021.763960.
[10] Lifton JJ, Carmignato S. Simulating the influence of scatter and beam hardening in dimensional computed tomography. Meas Sci Technol 2017;28. https://doi.org/10.1088/1361-6501/aa80b2.
[11] Lifton JJ, Malcolm AA. Estimating the product of the x-ray spectrum and quantum detection efficiency of a ct system and its application to beam hardening correction. Sensors 2021;21. https://doi.org/10.3390/s21093284.
[12] Reiter M, de Oliveira FB, Bartscher M, Gusenbauer C, Kastner J. Case study of empirical beam hardening correction methods for dimensional X-ray computed tomography using a dedicated multi-material reference standard. J Nondestr Eval 2019;38. https://doi.org/10.1007/s10921-018-0548-3.
[13] Borges de Oliveira F, Stolfi A, Bartscher M, De Chiffre L, Neuschaefer-Rube U. Experimental investigation of surface determination process on multi-material components for dimensional computed tomography. Case Stud Nondestruct Test Eval 2016;6:93–103. https://doi.org/10.1016/j.csndt.2016.04.003.
[14] Jansson A, Hermanek P, Pejryd L, Carmignato S. Multi-material gap measurements using dual-energy computed tomography. Precis Eng 2018;54:420–6. https://doi.org/10.1016/j.precisioneng.2018.07.012.
[15] Villarraga-Gómez H, Morse EP, Smith ST. Assessing the effect of penetration length variations on dimensional measurements with X-ray computed tomography. Precis Eng 2023;79:146–63. https://doi.org/10.1016/j.precisioneng.2022.10.001.
[16] Jiménez-Pacheco R, Ontiveros S, Yagüe-Fabra JA, Zanini F, Carmignato S, Albajez JA. Assessment of gradient-based algorithm for surface determination in multi-material gap measurements by X-ray computed tomography. Materials 2020; 13:1–11. https://doi.org/10.3390/ma13245650.
[17] Torralba M, Jiménez R, Yagüe-Fabra JA, Ontiveros S, Tosello G. Comparison of surface extraction techniques performance in computed tomography for 3D complex micro-geometry dimensional measurements. Int J Adv Manuf Technol 2018;97:441–53. https://doi.org/10.1007/s00170-018-1950-9.
[18] Yang X, Sun W, Giusca CL. An automated surface determination approach for computed tomography. NDT E Int 2022;131. https://doi.org/10.1016/j.ndteint.2022.102697.
[19] De Pastre MA, Thompson A, Quinsat Y, Albajez García JA, Senin N, Leach R. Polymer powder bed fusion surface texture measurement. Meas Sci Technol 2020; 31. https://doi.org/10.1088/1361-6501/ab63b1.
[20] Sun W, Giusca C, Lou S, Yang X, Chen X, Fry T, et al. Establishment of X-ray computed tomography traceability for additively manufactured surface texture evaluation. Addit Manuf 2022;50. https://doi.org/10.1016/j.addma.2021.102558.
[21] Curto M, Kao AP, Keeble W, Tozzi G, Barber AH. X-ray computed tomography evaluations of additive manufactured multimaterial composites. J Microsc 2022; 285:131–43. https://doi.org/10.1111/jmi.13034.
[22] Schmitt RH, Buratti A, Grozmani N, Voigtmann C, Peterek M. Model-based optimisation of CT imaging parameters for dimensional measurements on multimaterial workpieces. CIRP Ann 2018;67:527–30. https://doi.org/10.1016/j.cirp.2018.04.003.
[23] Dzullijah I., Songlin D., Shoujin S. Roughness Prediction For FDM Produced Surfaces, International Institute of Engineers; 2014. https://doi.org/10.15242/iie.e0214527.
[24] Buj-Corral I, Domínguez-Fernández A, Durán-Llucià R. Influence of print orientation on surface roughness in fused deposition modeling (FDM) processes. Materials 2019;12:3834. https://doi.org/10.3390/ma12233834.
[25] Computed tomography in dimensional metrology VDI/VDE 2630 Part 1.3: Accuracy of coordinate measuring machines characteristics and their testing. vol. 100. 2011.
[26] Villarraga-Gómez H, Smith ST. Effect of geometric magnification on dimensional measurements with a metrology-grade X-ray computed tomography system. Precis Eng 2022;73:488–503. https://doi.org/10.1016/j.precisioneng.2021.10.015.
[27] Kim K, Lee Y. Improvement of signal and noise performance using single image super-resolution based on deep learning in single photon-emission computed tomography imaging system. 2341–7 Nucl Eng Technol 2021;53. https://doi.org/10.1016/j.net.2021.01.011.
[28] Lou S, Brown SB, Sun W, Zeng W, Jiang X, Scott PJ. An investigation of the mechanical filtering effect of tactile CMM in the measurement of additively manufactured parts. Meas (Lond) 2019;144:173–82. https://doi.org/10.1016/j.measurement.2019.04.066.
[29] Conformity assessment - General requirements for the competence of proficiency testing providers (ISO/IEC 17043:2023). 2023.
[30] Geometrical product specifications (GPS). Coordinate measuring machines (CMM). Technique for determining the uncertainty of measurement. Part 3: Use of calibrated workpieces or measurement standards. (ISO 15530–3:2011). 2011.
[31] Computed tomography in dimensional measurement. VDI/VDE 2630 Part 2.1: determination of the uncertainty of measurement and the test process suitability of coordinate measurement systems with CT sensors. 2015.
[32] Villarraga-Gómez H, Lee CB, Smith ST. Dimensional metrology with X-ray CT: a comparison with CMM measurements on internal features and compliant structures. Precis Eng 2018;51:291–307. https://doi.org/10.1016/j.precisioneng.2017.08.021.
[33] Rodríguez-Sánchez Á, Thompson A, Körner L, Brierley N, Leach R. Review of the influence of noise in X-ray computed tomography measurement uncertainty. Precis Eng 2020;66:382–91. https://doi.org/10.1016/j.precisioneng.2020.08.004.
[34] Praniewicz M, Fox JC, Saldana C. Toward traceable XCT measurement of AM lattice structures: Uncertainty in calibrated reference object measurement. Precis Eng 2022;77:194–204. https://doi.org/10.1016/j.precisioneng.2022.05.010.
[35] Geometrical product specifications (GPS). Surface texture: Areal. Part 3: Specification operators (ISO 25178–3:2012). 2012.